JACS
JOURNAL OF THE AMERICAN CHEMICAL SOCIETY
Article
pubs.acs.org/JACS

Thiol–Ene Click Chemistry: Computational and Kinetic Analysis of the Influence of Alkene Functionality

Brian H. Northrop* and Roderick N. Coffey

Department of Chemistry, Wesleyan University, Middletown, Connecticut 06459, United States

Supporting Information

ABSTRACT: The influence of alkene functionality on the energetics and kinetics of radical initiated thiol–ene click chemistry has been studied computationally at the CBS-QB3 level. Relative energetics ($\Delta H°$, $\Delta H^{‡}$, $\Delta G°$, $\Delta G^{‡}$) have been determined for all stationary points along the step-growth mechanism of thiol–ene reactions between methyl mercaptan and a series of 12 alkenes: propene, methyl vinyl ether, methyl allyl ether, norbornene, acrylonitrile, methyl acrylate, butadiene, methyl(vinyl)silanediamine, methyl crotonate, dimethyl fumarate, styrene, and maleimide. Electronic structure calculations reveal the underlying factors that control activation barriers for propagation and chain-transfer processes of the step-growth mechanism. Results are further extended to predict rate constants for forward and reverse propagation and chain-transfer steps (k_P, k_{-P}, k_{CT}, k_{-CT}) and used to model overall reaction kinetics. A relationship between alkene structure and reactivity in thiol–ene reactions is derived from the results of kinetic modeling and can be directly related to the relative energetics of stationary points obtained from electronic structure calculations. The results predict the order of reactivity of alkenes and have broad implications for the use and applications of thiol–ene click chemistry.

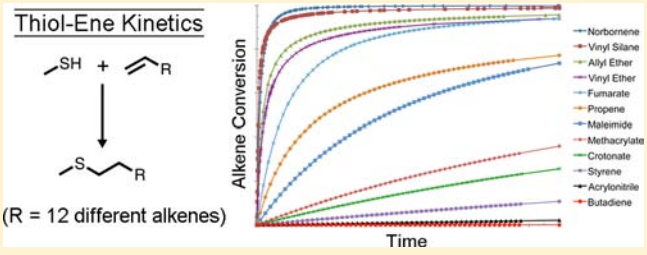

INTRODUCTION

The area of click chemistry[1] has seen rapid development across multiple areas of chemistry since Sharpless first codified the characteristics of click reactions in 2001. Reactions classified as "click" display several hallmarks that underlie their utility in chemical synthesis: high yields, short reaction times, wide functional group and solvent tolerance, regio- and chemoselectivity, insensitivity to O_2, few to no byproducts, facile purification, and high to 100% atom economy. Copper-catalyzed alkyne–azide click chemistry (CuAAC)[2] has emerged as the archetypical click reaction and has found applications throughout polymer[3] and dendrimer[4] chemistry, surface chemistry,[5] the preparation of biomedical libraries,[6] enzyme inhibitors,[7] cell derivitization,[8] and the synthesis of mechanically interlocked molecules.[9] A handful of other chemical reactions have also been recognized for their "spring-loaded" reactivity allowing them to be classified as click reactions, including but not limited to: oximine condensations, nucleophilic ring-opening of strained heterocyclic electrophiles (e.g., epoxides, aziridines), and Diels–Alder cycloadditions (e.g., maldimide–anthracene).[1a] The radical-initiated reaction of thiols with alkenes to give thioethers, while known for nearly a century, has recently experienced a resurgence in chemical synthesis and found increasing utility across multiple areas of chemistry, as it has proven to be an especially robust protocol in click chemistry.[10]

Thiol–ene reactions (Scheme 1) have been known[11] since the early 1900s. Many of the initial uses of thiol–ene chemistry focused on photo-curable polymers and resins for use in protective coatings and films.[12] Photoinduced thiol–ene polymerizations are known to rapidly and, often, quantitatively form highly uniform polymer networks with narrow glass transitions and easily tailorable mechanical properties. The step-growth mechanism[10,12,13] of thiol–ene polymerizations (Scheme 2) favors the formation of multiple low-molecular-

Scheme 1. Photoinitiated Thiol–Ene Click Chemistry

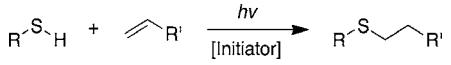

Scheme 2. Propagation, Chain-Transfer, and Chain Growth Processes That Are Operative within the Catalytic Cycle of Radical Initiated Thiol–Ene Click Chemistry ("I" Refers to Initiator)

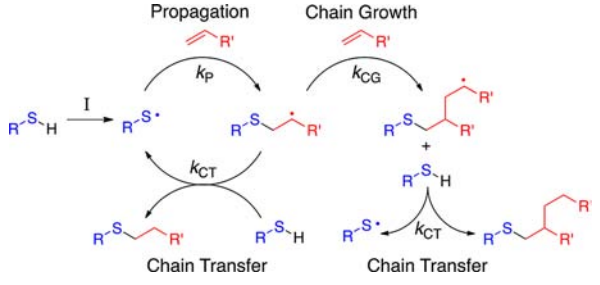

Received: June 5, 2012
Published: August 1, 2012

   dx.doi.org/10.1021/ja305441d | J. Am. Chem. Soc. 2012, 134, 13804–13817

weight species prior to gelation, resulting in high conversions at the gel point and largely homogeneous networks. These characteristics present several significant advantages over classical radical chain-growth polymerizations involving acrylates and methacrylates that often suffer from low pre-gel conversion and form more heterogeneous networks.

As the concepts and utility of click chemistry began to emerge in the early 2000s, the use of thiol−ene click chemistry has increased significantly and the applications of thiol−ene reactions have expanded far beyond photoinduced polymerization reactions. In the past 10 years alone, thiol−ene click chemistry has been utilized in multiple of areas in materials and bioorganic chemistry: e.g., dendrimer synthesis,[4d,e,14] nanoimprinting and nanostructured networks,[15] microfluidic devices,[16] surface patterning,[15a,17] electrooptical materials,[18] hydrogels,[19] polyhedral silsesquioxane chemistry,[20] micellular drug delivery,[21] and vaccine development.[22] Thiol−ene click chemistry offers particular advantages over CuAAC in some areas of bioconjugation chemistry as it avoids the use of noxious metal catalysts that can be toxic to living cells. Indeed, the selective and facile reactivity of thiols with maleimides has been one of the mainstays of bioconjugate chemistry for decades.[23] The subject of thiol−ene chemistry has been reviewed several times,[12,13] including recent applications of thiol−ene reactions in click chemistry.[10]

The typical mechanism of radical-catalyzed thiol−ene click chemistry involves the addition of a thiol across an alkene to give a thioether. While thioethers are predominantly observed, the mechanism can evolve along two different pathways following the generation of a thiyl radical (Scheme 2): (i) a step-growth pathway or (ii) a chain-growth pathway. Both mechanistic pathways begin with the same propagation step wherein a thiyl radical adds to an alkene, generating a carbon-centered radical intermediate. This radical intermediate can then undergo either a chain-transfer step by abstracting a hydrogen atom from another thiol (step-growth), or it can undergo a homopolymerization step by reacting with another equivalent of alkene (chain-growth). The step-growth path results in formation of a thioether product along with a new thiyl radical, which can then initiate another propagation step. The chain-growth path generates a new carbon-centered radical, which can subsequently follow a chain-transfer (shown) or another chain-growth pathway (not shown). Whether a step- or chain-growth pathway is followed depends on the relative kinetics of chain-transfer and homopolymerization which, in turn, depend on the nature of the carbon-centered radical and the alkene. Norbornene, for example, follows exclusively step-growth, while acrylates follow a combination of step- and chain-growth.[10c]

Experimental investigations[12,24−37] of photoinitiated click reactions between a given thiol and various alkenes have shown that the overall reaction rate varies considerably with the functionality of the alkene and, as such, the relationship between alkene structure and reactivity in thiol−ene reactions has been the subject of significant interest. Several experimental studies have reached a general consensus regarding the order of reactivity of alkenes with thiols, namely that norbornene and electron-rich alkenes (e.g., vinyl ether, allyl ether) are the most reactive, while electron-poor and conjugated alkenes (e.g., acrylonitrile, butadiene) are the least reactive.[10a,c] The particular order of reactivity, however, is still an open question and difficult to ascertain given differences in experimental conditions, variations in reactant structure, and the extremely rapid kinetics of the step-growth thiol−ene click mechanism.

In a series of recent studies Bowman and co-workers[31−33,35−38] have found that the most important factor governing the overall kinetics of thiol−ene polymerization is the ratio of the propagation rate (k_p) to the chain-transfer rate (k_{CT}). In general the relationship between k_P/k_{CT} and reaction order derived from experiment is

$$k_P/k_{CT}\begin{cases} \gg 1; & \text{rate} \propto [\text{SH}]^1 \\ \approx 1; & \text{rate} \propto [\text{SH}]^{1/2}[\text{C}=\text{C}]^{1/2} \\ \ll 1; & \text{rate} \propto [\text{C}=\text{C}]^1 \end{cases}$$

That is, when $k_P \gg k_{CT}$ the chain-transfer step is rate limiting and the overall rate is first order with respect to thiol concentration, and when $k_P \ll k_{CT}$ the propagation step is rate limiting and the overall rate is first order with respect to alkene concentration. In cases where $k_P \approx k_{CT}$ the overall rate is half order with respect to both thiol and alkene concentrations. Furthermore, the ratio k_P/k_{CT} has been shown[38] to influence the gel point of thiol−ene polymerizations, with higher k_P/k_{CT} ratios resulting in earlier gelation and lower ratios resulting in late gelation.

While the ratio of k_P/k_{CT} has provided significant insight into the kinetics of thiol−ene reactions, knowledge of individual reaction parameters (reaction and transition-state enthalpies and free energies) and individual rate constants (k_P and k_{CT}) is essential to optimizing synthetic protocols that utilize thiol−ene click reactions. An understanding of the factors that influence and control the barriers to propagation and chain-transfer is even more fundamental and would be of great synthetic utility. This is particularly the case with respect to complex reactions involving several thiols and/or alkenes. It is the goal of this research to elucidate and understand the factors that underlie the variations in thiol−ene reactivity with alkene structure.

Herein we report a thorough CBS-QB3[39] study of the mechanism of radical-initiated thiol−ene click chemistry. Methyl mercaptan is used as a model thiol, and its reactivity with a series of 12 alkenes (propene, methyl vinyl ether, methyl allyl ether, norbornene, acrylonitrile, methyl acrylate, butadiene, methyl(vinyl)silanediamine, methyl crotonate, dimethyl fumarate, styrene, and maleimide, Figure 1) is thoroughly

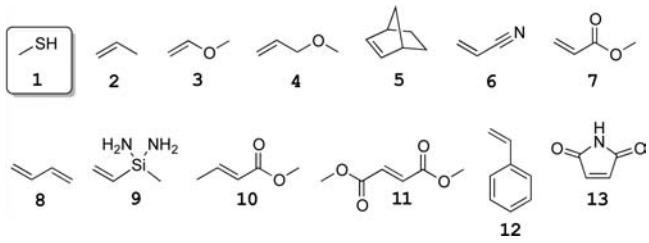

Figure 1. Chemical structures of the thiol and alkenes investigated in this study.

investigated. Calculated reaction and transition-state enthalpies and free energies are evaluated alongside the electronic properties of each alkene and radical intermediate to provide insight into the underlying factors that govern activation barriers to propagation and chain-transfer in the step-growth mechanism of thiol−ene reactions. Kinetic modeling of

dx.doi.org/10.1021/ja305441d | J. Am. Chem. Soc. 2012, 134, 13804−13817

computed reaction pathways supports experimental results and extends our understanding of the relationship between alkene functionality and the overall kinetics of thiol−ene click reactions.

RESULTS AND DISCUSSION

Reactions between alkane thiols and terminal alkenes to give linear thioethers are exothermic by approximately $\Delta H^\circ \approx -19$ kcal/mol. Experimental reaction enthalpies[40−47] of five representative examples of thiol−ene reactions between unsubstituted alkane thiols and alkenes are given in Table 1.

Table 1. Comparison of Experimental[a] and Calculated Reaction Enthalpies for a Series of Five Thiol−Ene Reactions and for the Homolytic Bond Cleavage of Methyl Mercaptan To Give Methyl Thiyl Radical and a Hydrogen Atom

Thiol	Alkene	Thioether	ΔH°_{Exp}[a]	$\Delta H^\circ_{CBS\text{-}QB3}$	Reference
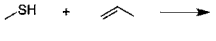			-18.8 (±0.6)	-19.3	40-42
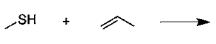			-20.8 (±0.6)	-21.7	40-42
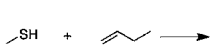			-18.8 (±0.9)	-19.8	40,43-44
			-18.9 (±0.2)	-18.8	41,44-45
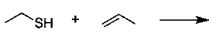			-18.4 (±0.2)	-18.7	43,46-47
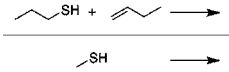			87.3 (±0.9)	86.9	48

[a]Reaction enthalpies were determined from experimental ΔH_f° values.[40−48] Values in parentheses represent experimental error.

These five reactions were used to benchmark the accuracy of computational methods used in this article. Compound CBS-QB3 methods were found to be in the closest agreement with experimental values, with a maximum deviation of ±1.0 kcal/mol and average deviations of ±0.5 kcal/mol. With experimental error taken into account the CBS-QB3 results deviate by a maximum ±0.2 kcal/mol. The bond dissociation energy of methyl mercaptan to give methyl thiyl radical and a hydrogen atom has been experimentally measured as requiring 87.3 ± 0.9 kcal/mol.[48] CBS-QB3 predicts a bond dissociation energy of 86.9 kcal/mol, in agreement within error of the experimental value. Density functional theoretical calculations at the B3LYP/6-311+G* level of theory consistently gave errors of greater than 4.0 kcal/mol for the same set of reactions as those in Table 1.

A generic potential energy surface corresponding to the radical initiated step-growth mechanism between methyl mercaptan and a generic alkene is shown in Figure 2. Transition-state energies for propagation ($\Delta E^\ddagger_P$) and chain-transfer ($\Delta E^\ddagger_{CT}$) are defined as shown in Figure 2. Also defined are ΔE°_{Int} and ΔE°_{Prod} corresponding to reaction energies for the formation of a carbon-centered radical intermediate following propagation and the formation of a thioether product following chain-transfer, respectively. As shown, Figure 2 does not take into account the initiation step necessary to form initial quantities of thiyl radical. Because a variety of photochemical and thermal initiators[49,50] can be used to catalyze thiol−ene reactions this study will focus on the principal steps of the thiol−ene step-growth mechanism—propagation and chain-transfer—and will not explicitly consider initiation. Chain growth processes (Scheme 2) were also not considered in the current study.

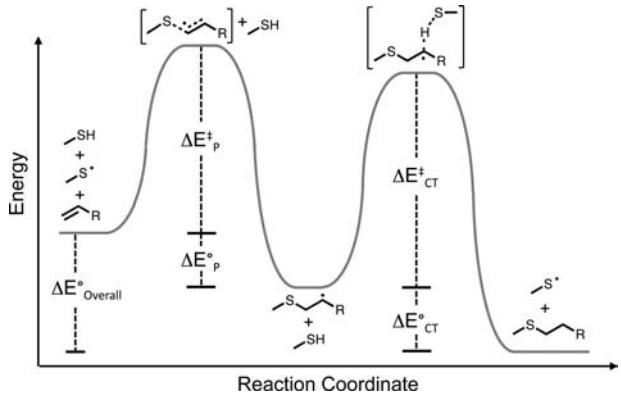

Figure 2. Generalized reaction profile for the step-growth mechanism of radical initiated thiol−ene click chemistry.

Potential energy surfaces for the radical initiated thiol−ene reactions between **1**• and each of the 12 alkenes **2**−**13** have been explored computationally with CBS-QB3 methods. The results are summarized in Table 2 and plotted graphically in Figure 3. All thiol−ene reactions studied are exothermic, with overall reaction enthalpies ranging from −15.3 kcal/mol to −25.4 kcal/mol and free energies ranging from −4.5 kcal/mol to −13.3 kcal/mol. While the 12 reactions studied are all thermodynamically favorable, Table 2 shows that individual thiol−ene reaction energetics vary considerably with alkene functionality. Activation enthalpies for the addition of thiyl radical **1**• to alkenes **2**−**13** ($\Delta H^\ddagger_P$) are predicted to be negative, in agreement with what has been found experimentally by Sivertz and co-workers.[26−28] By contrast, $-T\Delta S^\ddagger_P$ is strongly positive (9.6−11.7 kcal/mol) for all propagation transition states. It follows that as thiyl radical **1**• approaches alkenes **2**−**13**, the slope of the potential enthalpy surface (ΔH_P) is negative whereas the slope of the potential entropy surface ($-T\Delta S_P$) is positive. The point where the negative slope of ΔH_P equals the positive slope of $-T\Delta S_P$ defines the transition state of the overall free energy potential surface ($\Delta G^\ddagger_P$). Propagation transition-state free energies for the series of 12 alkenes all fall within a range of 3.4 kcal/mol from a low of $\Delta G^\ddagger_P$ = 6.8 kcal/mol (butadiene, **8**) to a high of $\Delta G^\ddagger_P$ = 10.2 kcal/mol (maleimide, **13**).

The formation of a carbon-centered radical intermediate following propagation varies from being strongly exergonic (ΔG°_P = −7.8 kcal/mol, butadiene, **8**) to slightly endergonic (ΔG°_P = 2.1 kcal/mol, vinyl ether, **3**). It is known[13,26−28,34] that thiyl radical addition to alkyl and electron rich alkenes is a thermodynamically reversible process, which is supported by results in Table 2. Chain-transfer transition-state free energies as defined in Figure 2 show nearly 3 times as great of variation as propagation transition-state free energies, ranging from $\Delta G^\ddagger_{CT}$ = 7.8 kcal/mol (vinyl silane, **9**) to $\Delta G^\ddagger_{CT}$ = 17.3 kcal/mol (butadiene, **8**). Figure 3 plots the energetics of stationary points along the step-growth mechanism of all 12 thiol−ene reactions on the same relative scale with each starting thiyl/ene combination taken as 0.0 kcal/mol. While individual stationary point free energies may not each be easily discernible in Figure 3, variations in reaction coordinate diagrams are more clearly pronounced when collective free energy data are plotted on the same relative scale.

The relative rates of propagation and chain-transfer depend on the nature of the thiol and the alkene involved, as well as the nature of the thiyl radical and carbon-centered radical

dx.doi.org/10.1021/ja305441d | J. Am. Chem. Soc. 2012, 134, 13804−13817

Table 2. Calculated[a] Reaction and Transition-State Enthalpies ($\Delta H°$, $\Delta H^{‡}$) and Free Energies ($\Delta G°$, $\Delta G^{‡}$) for Propagation and Chain-Transfer Processes Involving Thiol 1 and Alkenes 2−13

	propagation				chain-transfer					
	transition state		intermediate		transition state		product		overall	
alkene	$\Delta H^{‡}_{P}$	$\Delta G^{‡}_{P}$	$\Delta H°_{P}$	$\Delta G°_{P}$	$\Delta H^{‡}_{CT}$	$\Delta G^{‡}_{CT}$	$\Delta H°_{CT}$	$\Delta G°_{CT}$	$\Delta H°_{rxn}$	$\Delta G°_{rxn}$
2	−0.6	9.2	−8.8	1.4	−0.2	10.2	−10.5	−9.1	−19.3	−7.7
3	−1.8	8.0	−7.9	2.1	−2.9	8.2	−7.4	−6.6	−15.3	−4.5
4	−1.4	9.1	−8.8	1.6	−1.8	8.4	−13.1	−11.5	−21.9	−9.9
5	−3.4	6.9	−14.5	−3.2	−1.0	9.8	−11.0	−10.1	−25.4	−13.3
6	−0.7	7.7	−16.4	−5.3	4.6	14.8	−3.3	−2.9	−19.6	−8.2
7	−2.5	8.6	−14.3	−3.2	2.3	12.9	−5.3	−5.4	−19.7	−8.6
8	−2.8	6.8	−18.6	−7.8	7.2	17.3	2.7	3.1	−15.9	−4.7
9	−2.2	8.0	−10.4	0.4	−3.1	7.8	−10.6	−10.0	−21.0	−9.6
10	−2.4	9.0	−13.1	−1.4	2.3	13.1	−5.1	−4.7	−18.3	−6.1
11	−3.2	8.5	−12.9	−1.2	0.2	11.1	−7.3	−7.1	−20.2	−8.3
12	−1.7	8.6	−16.6	−4.5	3.9	13.8	−1.7	−1.5	−18.3	−6.0
13	−1.0	10.2	−14.2	−2.5	1.8	12.1	−6.1	−6.1	−20.3	−8.6

[a]Energies (CBS-QB3) are reported in kcal/mol in the gas phase at 298.15 K, 1.0 atm, and defined as shown in Figure 2.

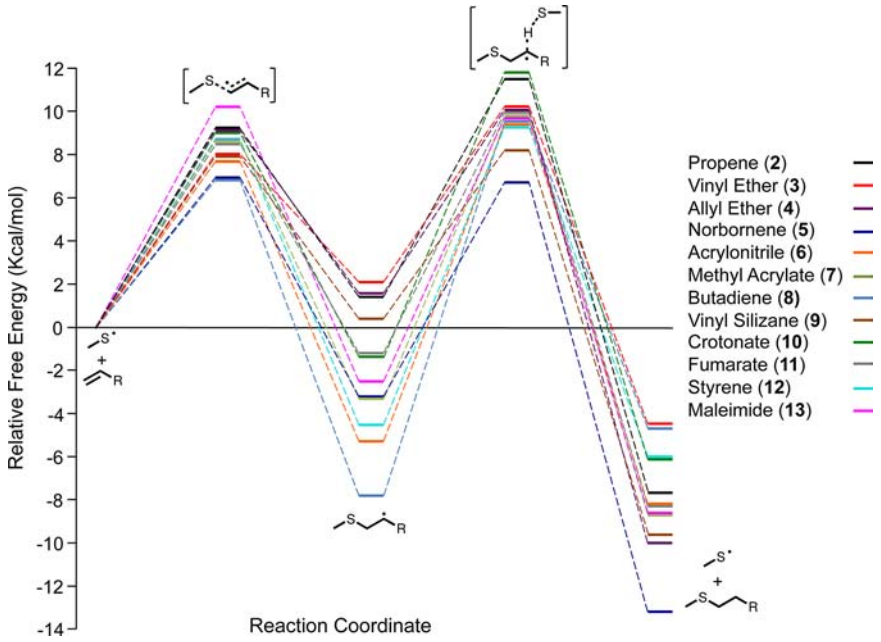

Figure 3. Relative free energies of stationary points along the step-growth thiol−ene reactions between methyl mercaptan and alkenes **2**−**13**. Computed reaction and transition-state free energies used to generate this plot are given in Table 2.

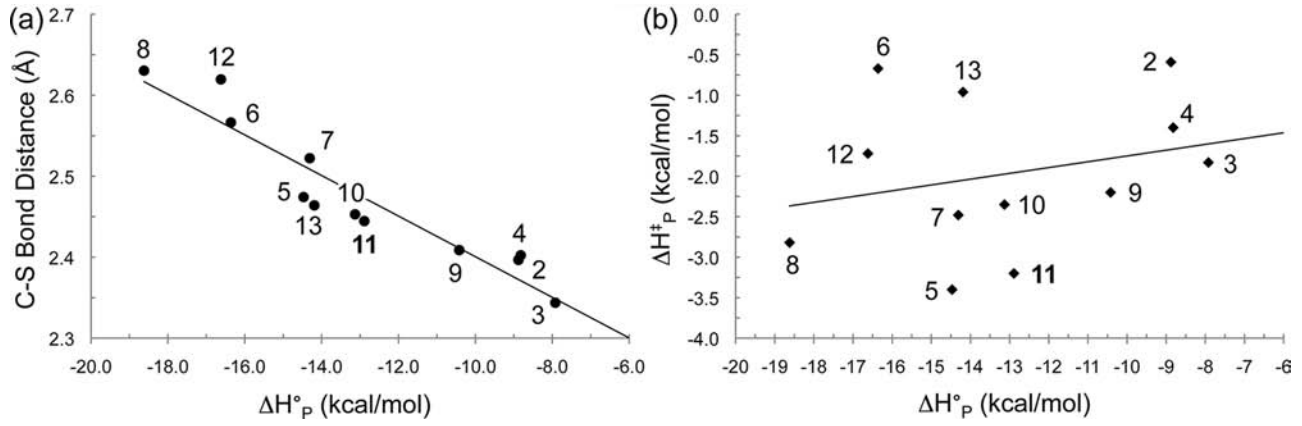

Figure 4. (a) Plot of C−S bond distance in each propagation step transition structure versus reaction enthalpy (R^2 = 0.90). (b) Plot of propagation step transition-state enthalpy versus reaction enthalpy (R^2 = 0.08) for the addition of thiyl radical **1**• to alkenes **2**−**13**.

dx.doi.org/10.1021/ja305441d | J. Am. Chem. Soc. 2012, 134, 13804−13817

intermediates. It has been proposed[10a,b,33] that the rate of propagation (k_P) is controlled by the electron density of the reacting ene while the rate of chain-transfer (k_{CT}) is controlled by the stability of the carbon-centered radical intermediate. Knowledge of activation parameters ($\Delta H^{\ddagger}$, $\Delta G^{\ddagger}$) for propagation and chain-transfer provides direct insight into their kinetics. Computational studies presented herein have enabled us to investigate, in detail, the relationships between alkene structure and activation barriers to propagation and chain-transfer in thiol−ene click reactions.

Thiyl Addition to Alkenes: The Propagation Step. The addition of carbon-centered radicals to alkenes has been extensively studied both experimentally[51−53] and theoretically,[54] and the geometric and energetic factors controlling rates of carbon-centered radical addition to alkenes have been reviewed several times.[51−53] Cumulative research has found that activation barriers for the addition of carbon-centered radicals to alkenes are influenced by varying combinations of (i) steric effects, (ii) reaction enthalpy, (iii) polar effects, and (iv) alkene singlet−triplet gap. Less is known about the details of thiyl radical additions to alkenes. It may be expected, as a first approximation, that thiyl radicals will follow similar trends as carbon-centered radicals.

As shown in Table 2, all 12 propagation steps are exothermic, as a relatively weak C−C π bond is replaced with a stronger C−S σ bond. A plot of reaction enthalpy versus forming C−S bond distance in each propagation transition state is shown in Figure 4a. The approximately linear correlation (R^2 = 0.90) is in accordance with an early transition state, as would be expected by the Hammond postulate.[55] Thiyl radical addition to butadiene (**8**), for example, is the most exothermic (ΔH_P = −18.6 kcal/mol), exhibits the longest C−S separation in the transition state (2.630 Å), and has the lowest free energy of activation ($\Delta G^{\ddagger}_P$ = 6.8 kcal/mol) of the 12 alkenes investigated. This result is easily rationalized given the relatively high electron density[56] of butadiene and the favorability of forming a resonance-stabilized allylic radical intermediate. However, attempts to generalize the influence of alkene electron density and/or resonance-stabilization of the carbon-centered radical intermediate across the series of 12 alkenes fail. Maleimide (**13**) and acrylonitrile (**6**), for example, both have low alkene electron density and are able to stabilize, through resonance, the carbon-centered radical formed following propagation, yet the propagation free energy barrier of maleimide is the highest of the series investigated ($\Delta G^{\ddagger}_P$ = 10.2 kcal/mol) while the propagation free energy barrier of acrylonitrile is the third lowest ($\Delta G^{\ddagger}_P$ = 7.7 kcal/mol). Propagation free energy barriers for eight of the nine remaining alkenes (**2**−**4**, **7**, **9**−**12**) all fall within a range of 1.1 kcal/mol ($\Delta G^{\ddagger}_P$ = 8.0−9.1 kcal/mol) despite notable variations in alkene electron density and conjugation. Norbornene (**5**) is a particularly notable outlier because its low propagation free energy barrier[57] of $\Delta G^{\ddagger}_P$ = 6.9 kcal/mol is largely the result of released ring strain. It is clear form the results summarized in Table 2 that a direct correlation between propagation activation barrier and alkene electron density or conjugation cannot be made.

A plot of propagation transition-state enthalpy versus reaction enthalpy (Figure 4b) shows no observable correlation. This indicates that an Evans−Polanyi relationship,[58] eq 1, does

$$E_a = \text{constant} + \alpha \Delta H^{\circ} \quad (1)$$

not exist for this series of thiyl−ene propagation reactions.The correlation between enthalpy and the *location* of the transition-state barrier but lack of correlation between enthalpy and the *height* of the transition-state barrier is supportive of a curve-crossing model[53,59,60] of barrier formation (Figure 5). As shown

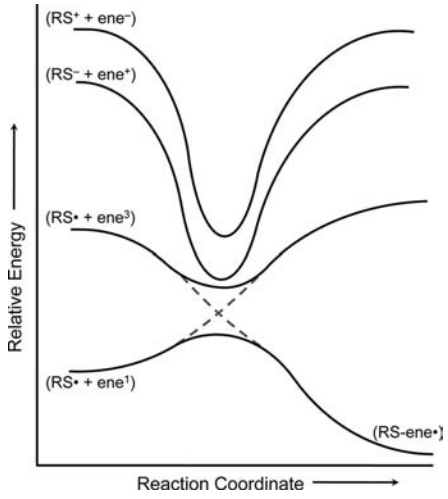

Figure 5. General schematic of a curve-crossing model (also known as a state correlation diagram) for the addition of a thiyl radical to alkenes. Higher energy nonpolar configuration ($RS^{\bullet}$ + ene^3) and polar configurations (RS^- + ene^+) and (RS^+ + ene^-) may mix with the lower energy singlet configuration ($RS^{\bullet}$ + ene^1) to reduce the propagation step transition-state barrier.

in Figure 5 the overall activation barrier for the addition of a radical to an alkene can be influenced by four electronic configurations: the two nonpolar configurations ($RS^{\bullet}$ + ene^1) and ($RS^{\bullet}$ + ene^3) as well as the two polar charge-transfer configurations (RS^- + ene^+) and (RS^+ + ene^-). Contributions from nonpolar configurations depend directly on the alkene singlet−triplet gap while polar charge-transfer configurations are related to reactant ionization potentials and electron affinities as well as Coulombic attraction between the ionized alkene and radical in the transition state. Mixing of one or more of these higher energy configurations with the lowest energy singlet conformation can lead to a lowering of the overall activation barrier. When triplet and charge-transfer configurations are significantly above the ground-state singlet configuration no mixing is observed and activation enthalpies tend to correlate with reaction enthalpies. The null correlation of Figure 4b suggests that triplet and/or charge-transfer configurations likely influence the propagation step activation barriers between thiyl radical $\mathbf{1}^{\bullet}$ and alkenes **2**−**13**. The extent of these effects will vary with alkene substitution and require further investigation of the electronic properties of alkenes **2**−**13**.

Energies of charge-transfer configurations (Table 3) were determined from computed adiabatic ionization potentials and electron affinities of structures **1**−**13**. The charge-transfer configuration (RS^- + ene^+) was found to be lower energy than configuration (RS^+ + ene^-) for each alkene investigated, indicating electrophilic behavior of the thiyl radical. Electrophilic behavior of thiyl radical $\mathbf{1}^{\bullet}$ is further supported by the positive charge-transfer to alkenes **2**−**13** in the transition state ($\delta^{\ddagger}$). Coulombic stabilization of the (RS^- + ene^+) configuration can be approximated by the electrostatic attraction between two point-charges separated by the C−S distance in each

dx.doi.org/10.1021/ja305441d | J. Am. Chem. Soc. 2012, 134, 13804−13817

Table 3. Energies[a] of Charge-Transfer Configurations in the Reaction between Thiyl Radical 1• and Alkenes 2−13, along with C−S Bond Distances,[b] Point-Charge Approximations of Coulombic Attraction at Each Transition-State Geometry, Lowest Energy Coulombically Stabilized Charge-Transfer Configuration E_{CT}, Alkene Singlet−Triplet Gaps, and Amount of Charge-Transfer[c] from Thiyl 1• to Alkenes 2−13 in the Transition State

alkene	$(RS^- + ene^+)$	$(RS^+ + ene^-)$	C−S‡	C[a]	E_{CT}	ΔE_{ST}	$\delta^‡$
acrylonitrile (**6**)	9.0	10.1	2.566	5.6	3.4	2.6	0.096
methacrylate (**7**)	8.2	10.1	2.522	5.7	2.5	2.6	0.139
maleimide (**13**)	8.2	8.8	2.464	5.8	2.4	3.1	0.131
fumarate (**11**)	8.3	9.0	2.445	5.9	2.4	2.6	0.167
crotonate (**10**)	7.8	10.3	2.453	5.9	1.9	2.8	0.212
propene (**2**)	7.9	12.1	2.397	6.0	1.9	2.9	0.199
allyl ether (**4**)	7.8	11.1	2.402	6.0	1.8	2.9	0.205
butadiene (**8**)	7.2	10.6	2.630	5.5	1.7	2.5	0.126
norbornene (**5**)	7.0	11.5	2.474	5.8	1.1	3.4	0.292
styrene (**12**)	6.6	10.2	2.620	5.5	1.1	2.5	0.143
vinyl ether (**3**)	7.1	11.8	2.344	6.1	0.9	3.0	0.246
silane (**9**)	6.9	10.9	2.409	6.0	0.9	2.8	0.140

[a]All energies are given in eV. [b]Bond distances are given in Å. [c]Mulliken charges.

transition state (Table 3, columns 3 and 4). It should be noted that this estimation serves as an upper limit of the Coulombic attraction given that ionized alkenes and thiyl radicals are not point charges and varying extents of charge delocalization will occur. The lowest energy charge-transfer configuration is therefore approximated as $E_{CT} = [(RS^- + ene^+) - C]$ for each alkene and is given in column 5 of Table 3. Alkenes **2**−**13** are listed in order of decreasing influence of charge-transfer on propagation step activation barriers. As can be seen from the table, polar effects are predicted to have little to no influence on activation barriers for the addition of a thiyl radical to electron poor alkenes such as acrylonitrile (**6**), methacrylate (**7**), maleimide (**13**), and fumarate (**11**). The high ionization potentials of electron-poor alkenes render formation of the $(RS^- + ene^+)$ charge-transfer configuration too energetically costly to influence the ground-state activation barrier. On the other hand, polar effects are predicted to contribute to the lowering of activation barriers for the addition of a thiyl radical to electron-rich alkenes such as norbornene (**5**), styrene (**12**), vinyl ether (**3**), and vinyl silane (**9**). These predictions are in general agreement with experimentally measured rates of propagation steps between alkyl thiols and substituted alkenes.

Computed singlet−triplet gaps for alkenes **2**−**13** are given in column 6 of Table 3. The configuration $(RS^• + ene^3)$ is generally less stable than stabilized charge-transfer configurations, i.e., $\Delta E_{ST} > E_{CT}$. Consequently, it can be expected that the influence of alkene triplet configurations on propagation step activation barriers will be small relative to the influence of polar effects. There are, however, exceptions to this observation. In particular the triplet configuration of acrylonitrile (**6**) is predicted to be 0.8 eV *more* stable than the lowest energy charge-transfer configuration. The low-energy acrylonitrile triplet configuration ($CH_3S^•$ + acrylonitrile^3) can therefore be expected to have a greater influence on the activation barrier for addition of **1**• to acrylonitrile than polar charge-transfer configurations. Triplet energies of methacrylate (**7**) and fumarate (**11**) are each within 0.2 eV of their lowest energy charge-transfer configurations and may influence their respective propagation step activation barriers as well. Triplet energies for all other alkenes investigated are each 0.7−2.2 eV greater than charge-transfer configurations and expected to be of little influence.

With the series of alkenes studied it is not possible to draw a direct correlation between the propagation step activation barrier and any single structural or electronic property of alkenes **2**−**13**. To account for the varying influence of charge-transfer effects in radical additions to double bonds Fisher and Radom have developed[53] a modified Evans−Polanyi expression (eqs 2 and 3) wherein polar charge-transfer effects are taken

$$\Delta E^‡ = (11.95\ \text{kcal/mol} + 0.22\Delta E^\circ)F_e \quad (2)$$

$$F_e = 1 - \exp(-[(E_{IP}(\text{alkene}) - E_{EA}(\text{radical}) - C)/\gamma)^2]) \quad (3)$$

into account using a multiplicative polar factor rather than simply an additive term. By including a treatment for the stabilizing influence of polar charge-transfer configurations Fisher and Radom have shown that a nonlinear relationship exists between reaction enthalpies and activation barriers for the addition of carbon-centered radicals to alkenes that is generally well-treated using eqs 2 and 3. This analysis was adapted to the addition of thiyl radical **1**• to alkenes **2**−**13** and the results are shown in Figure 6. Energies of charge-transfer configurations $(RS^- + ene^+)$ are plotted against the free energy of activation $(\Delta G^‡)$ divided by reaction energy term (11.95 kcal/mol + 0.22ΔG°). The solid line in Figure 6 corresponds to the function F_e (eq 3) that accommodates the data by relating reaction and activation energies to charge-transfer stabilization (E_{IP}(ene) − $E_{EA}(RS^•)$ − $C = E_{CT}$) and an interaction parameter γ. In the absence of any charge-transfer effects the plot in Figure 3 would be a horizontal line with a y-intercept of 1.0.

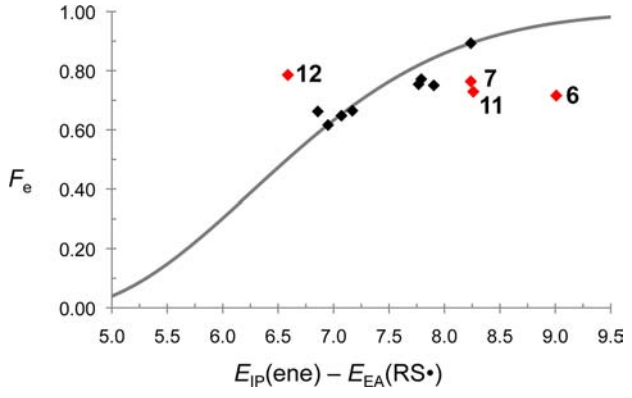

Figure 6. Plot of the energy of polar charge-transfer configurations $(RS^- + ene^+)$ (eV) versus electrophilic polar factor $F_e = (\Delta G^‡)/(11.95$ kcal/mol + 0.22ΔG°) for the addition of thiyl radical **1**• to alkenes **2**−**13**. The inclusion of nonlinear polar effects helps explain the relationship between propagation step activation energies and reaction energies for 8 of the 12 alkenes studied. The four outliers—styrene (**12**), fumarate (**11**), methacrylate (**7**), and acrylonitrile (**6**)—can be accounted for by considering resonance stabilization and the influence of nonpolar triplet configurations $(RS^• + ene^3)$.

dx.doi.org/10.1021/ja305441d | J. Am. Chem. Soc. 2012, 134, 13804−13817

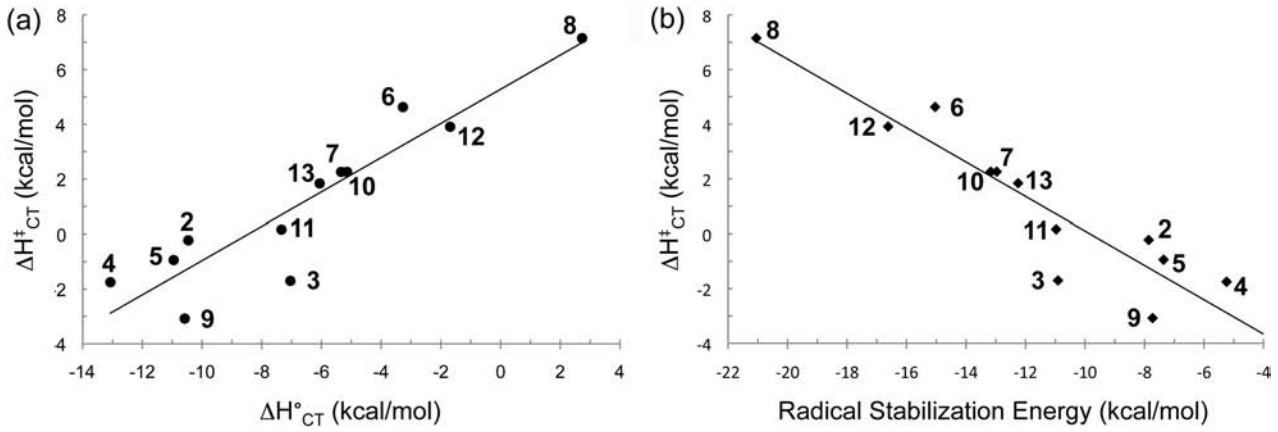

Figure 7. (a) Plot of reaction enthalpy versus transition-state enthalpy for the abstraction of a hydrogen atom from methyl mercaptan (**1**) by carbon-centered radical intermediates **2**–**13** (R^2 = 0.83). (b) Linear relationship between the radical stabilization energy of carbon-centered radicals **2**–**13** and chain-transfer transition-state enthalpies (R^2 = 0.86). Carbon-centered radicals arising from vinyl ether (**3**) and vinyl silane (**9**) are outliers in each plot and can be accounted for by stabilizing orbital interactions.

This, however, is not the case. Instead there is a general trend toward lower activation barriers with lower energy charge-transfer configurations, as would be expected from the curve-crossing model.

Data points for 8 of the 12 alkenes studied are accommodated well by the model; however, the four data points highlighted in red are not. These four most significant outliers correspond to styrene (**12**), fumarate (**11**), methacrylate (**7**), and acrylonitrile (**6**). It is known that polar effects are typically overestimated for phenyl-substituted alkenes[53] on account of increased charge delocalization through the aromatic ring. A point charge estimation of the styrene cation is therefore a poor model and leads to an overestimation of Coulombic attraction, hence styrene lies significantly above the curve. The poor agreements in the cases of fumarate (**11**), methacrylate (**7**), and acrylonitrile (**6**), on the other hand, likely result from the fact that the model does not take into account the influence of the alkene triplet configuration ($RS^{\bullet}$ + ene^3). As noted earlier the energy of the alkene triplet configuration is significantly higher than the lowest energy, Coulombically stabilized charge-transfer configuration for all but three alkenes: fumarate (**11**), methacrylate (**7**), and acrylonitrile (**6**) (see Table 3). It is therefore expected that the relatively low lying nonpolar triple configurations ($RS^{\bullet}$ + ene^3) of fumarate, methacrylate, and acrylonitrile are able to mix with their ground-state reaction coordinate, lowering propagation step activation barriers below what would be expected from analysis of charge-transfer configurations alone. Given that the triplet configuration of acrylonitrile is 0.8 eV more stable than its lowest energy charge-transfer configuration it would be predicted that acrylonitrile (**6**) would be the greatest outlier in Figure 6, which indeed it is.

Overall, computational investigations of the addition of thiyl radical $\mathbf{1}^{\bullet}$ to alkenes **2**–**13** suggest that propagation step activation barriers depend on a number of factors rather than a single predominant parameter. Of primary importance is the extent of mixing of charge-transfer and/or triplet configurations (RS^- + ene^-) and ($RS^{\bullet}$ + ene^3), respectively, with the ground-state configuration ($RS^{\bullet}$ + ene^1). Relative energies, and thus influence, of charge-transfer and triplet configurations depend on a mixture of electronic properties of each alkene and vary significantly across the series of 12 alkenes investigated. While propagation activation barriers cannot be correlated to any one property or characteristic of a given alkene, a greater understanding of activation energetics can be obtained with knowledge of ion energetics, singlet–triplet gaps, transition-state structures, and reaction enthalpies. Computational investigations are particularly useful in this regard given the difficulty of obtaining experimental transition-state structural parameters.

Thiol Hydrogen Atom Abstraction: The Chain-Transfer Step. Following propagation, radical-initiated thiol–ene click reactions undergo a chain-transfer step wherein the newly formed carbon-centered radical abstracts a thiol hydrogen atom (Scheme 2). Chain-transfer free energy barriers obtained from CBS-QB3 calculations (Table 1) range from a low of 7.8 kcal/mol in the case of vinyl silane (**9**) to a high of 17.3 kcal/mol for butadiene (**8**). This range of 9.5 kcal/mol is notably greater than the range in propagation step free energy barriers ($\Delta G^{\ddagger}_{P}$ = 6.8–10.2 kcal/mol). The increased variation in chain-transfer free energy barriers is largely reflective of the differences in propagation step reaction energies, which range from exergonic (ΔG° = −7.8 kcal/mol, butadiene **8**) to endergonic (ΔG° = 2.1 kcal/mol, vinyl ether **3**). It is reasonable to conclude that carbon-centered radical intermediates formed following propagation are more dissimilar than their respective starting alkenes and, therefore, are more likely to influence overall reaction energetics.

As can be seen in Figure 7a, activation enthalpies ($\Delta H^{\ddagger}$) for chain-transfer correlate well with reaction enthalpies (ΔH°). Polar charge-transfer effects are therefore not expected to influence chain-transfer activation energetics. Strong correlations also exist between reaction enthalpies and bond lengths for both the breaking S–H and forming C–H bonds in the chain-transfer transition-state structures (see Figure S2 of the Supporting Information).

Bowman et al. have suggested[33] that the rate of chain-transfer (k_{CT}) is correlated with the stability of the carbon-centered radical generated following propagation. Radical stabilization energies relative to methyl radical were calculated for each carbon-centered radical intermediate according to the isodesmic reaction

$$RH + CH_3^{\bullet} \rightarrow R^{\bullet} + CH_4 \quad (4)$$

Resulting radical stabilization energies ranged from −5.2 kcal/mol (allyl ether **4**) to −21.1 kcal/mol (butadiene **8**). Computed

dx.doi.org/10.1021/ja305441d | J. Am. Chem. Soc. 2012, 134, 13804–13817

radical stabilization energies for the 12 carbon-centered radicals studied do show an approximately linear correlation with chain-transfer activation barriers (Figure 7b), supporting the theory put forth by Bowman. While the correlation is reasonable (R^2 = 0.86) there are two notable outliers: carbon-centered radicals resulting from thiyl addition to vinyl ether (**3**) and vinyl silane (**9**), which deviate in the direction of higher than expected radical stabilization energies. These are the only two intermediates with a heteroatom alpha to the carbon-centered radical, which is suggestive that α-heteroatoms may play a factor in the stability of carbon-centered radical intermediates derived from vinyl ether (**3**) and vinyl silane (**9**). NBO analysis of the SOMO orbitals of carbon-centered radicals arising from **3** and **9** reveal significant orbital overlap between the carbon-centered radical and the α-oxygen atom of **3** and α-silicon atom of **9** (Figure 8). It is known that oxygen atoms can act as

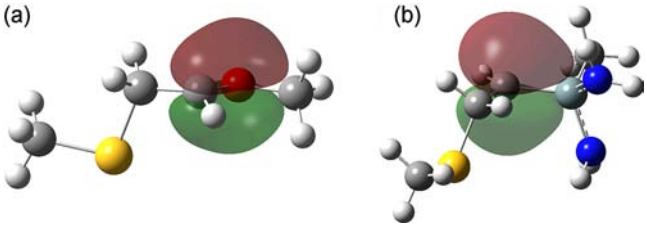

Figure 8. SOMOs of radical intermediates formed following the addition of thiyl radical **1**$^{\bullet}$ to (a) vinyl ether **3** and (b) vinyl silane **9**, indicating stabilizing orbital overlap between the carbon-centered radical and the α-oxygen atom of **3** and the α-silicon atom of **9** due to mesomeric and d_π–p_π interactions, respectively.

mesomeric electron-donating groups to stabilize α radicals.[61,62] Silicon has been shown to stabilize α radicals through the delocalization of the unpaired electron of the carbon-centered radical into a 3d orbital of silicon (d_π–p_π bonding).[62,63] These stabilizing orbital interactions help explain the deviation of vinyl ether (**3**) and vinyl silane (**9**) toward greater radical stabilization energies observed in Figure 7b. Similar stabilizing orbital interactions could not be observed by NBO analysis for any of the other 10 carbon-centered radicals investigated. It is worth noting that vinyl ether radical **3** and vinyl silane radical **9** are also the two most significant outliers in the plot of reaction enthalpy versus activation enthalpy (Figure 7a). It is likely that these deviations from a linear correlation can also be accounted for by stabilizing orbital interactions that decrease the reaction enthalpy of chain-transfer (ΔH°_{CT}). When vinyl ether (**3**) and vinyl silane (**9**) are removed from both plots of Figure 7, the R^2 values of each plot increase to 0.96.

Reaction Rates and Kinetic Modeling. Of key importance to the application and optimization of thiol–ene click chemistry are the relative rates of propagation (k_P) and chain-transfer (k_{CT}).[32−38] Individual kinetic parameters are especially influential in photoinitiated thiol–ene polymerizations where the ratio of k_P/k_{CT} affects the reaction order with respect to thiol and alkene concentrations as well as the polymer gelation time and gel point, which ultimately affect overall mechanical properties. While the electronic structure calculations presented above are able to help elucidate the fundamental factors that control the energetics of propagation and chain-transfer for reactions of thiyl **1**$^{\bullet}$ with alkenes **2**–**13**, kinetic modeling of the addition of thiyl radicals to substituted alkenes provides a more complete understanding of their overall reactivity.

Reaction and activation enthalpies and free energies presented in Table 2 were used to calculate rate constants for propagation and chain-transfer in thiol–ene reactions between **1** and alkenes **2**–**13**. For completeness both forward and reverse rate constants were calculated as the addition of thiyl radicals to electron rich alkenes is known to be reversible.[13,26−28,34,64] Rate constants were calculated at 298.15 K using conventional activated complex theory:[65]

$$A = X\frac{k_B T}{hc^\circ}\, e^{(1-\Delta n^\ddagger)}\, e^{\Delta S^\ddagger/R} \quad (5)$$

$$E_a = \Delta H^\ddagger + (1 - \Delta n^\ddagger)RT \quad (6)$$

$$k(T) = A\, e^{-E_a/RT} \quad (7)$$

where k_B is the Boltzmann constant, T is the temperature, h is Planck's constant, c° is the standard-state concentration (taken here to be 1.0 M), $\Delta n^\ddagger$ is the change in the number of particles between the reactant(s) and the transition state, $\Delta S^\ddagger$ and $\Delta H^\ddagger$ are the calculated changes in entropy and enthalpy between the reactant(s) and transition state, E_a is the activation energy, A is

Table 4. Rate Constants for Forward[a] and Reverse[b] Radical-Initiated Propagation and Chain-Transfer Steps between Thiol 1 and Alkenes 2–13 Obtained from Computed Reaction Energetics (Table 3) as Well as Theoretical and Experimental[c] Ratios of Forward Propagation and Chain-Transfer Rate Constants (k_P/k_{CT}) for Each Alkene

	propagation (k_P)		chain-transfer (k_{CT})		k_P/k_{CT}	
alkene[d]	forward	reverse	forward	reverse	theory	experiment
butadiene (**8**)	6.5×10^7	1.3×10^2	1.4×10^0	2.6×10^2	47,000,000	1,500,000[c]
acrylonitrile (**6**)	1.4×10^7	1.0×10^2	9.3×10^1	7.5×10^{-1}	150,000	
styrene (**12**)	3.1×10^6	1.3×10^3	5.0×10^2	4.0×10^1	6,100	800,000[e]
methacrylate (**7**)	3.2×10^6	1.5×10^4	2.1×10^3	2.3×10^{-1}	1,500	13[f]
crotonate (**10**)	1.7×10^6	1.6×10^5	1.5×10^3	5.1×10^{-1}	1,100	
norbornene (**5**)	5.2×10^7	2.5×10^5	3.8×10^5	1.5×10^{-2}	140	1.0[f]
fumarate (**11**)	3.5×10^6	4.6×10^5	4.2×10^4	2.9×10^{-1}	83	
maleimide (**13**)	2.1×10^5	3.1×10^3	8.2×10^3	1.3×10^{-1}	26	
propene (**2**)	1.1×10^6	1.1×10^7	2.3×10^5	4.7×10^{-2}	5.0	5.0[c]
vinyl ether (**3**)	8.0×10^6	2.7×10^8	6.1×10^6	1.3×10^1	1.3	1.2[f]
vinyl silane (**9**)	9.0×10^6	1.3×10^7	1.3×10^7	5.8×10^{-1}	0.7	0.2[f]
allyl ether (**4**)	1.2×10^6	1.7×10^7	4.2×10^6	1.6×10^{-2}	0.3	10[f]

[a]In M^{-1} s^{-1}. [b]In s^{-1}. [c]Reference 24. [d]Alkenes are listed in order of highest to lowest predicted k_P/k_{CT} ratio. [e]Reference 27. [f]Reference 33.

dx.doi.org/10.1021/ja305441d | J. Am. Chem. Soc. 2012, 134, 13804–13817

the Arrhenius pre-exponential factor, and X is the transmission coefficient to account for tunneling and recrossing effects (for simplicity taken to be unity). Because CBS-QB3 calculations were performed in the gas phase, rate constants calculated from CBS-QB3 reaction energetics should also be considered gas phase. Table 4 lists the forward and reverse rate constants for propagation and chain-transfer steps between thiol **1** and alkenes **2**−**13**. Complete tables of calculated transition-state entropies, pre-exponential factors, and activation energies are provided in the Supporting Information. Forward propagation rate constants range from 10^5 to 10^7 M^{-1} s^{-1}, whereas forward chain-transfer rate constants show much greater variation, ranging from 10^0 to 10^7 M^{-1} s^{-1}. These variations in rate mirror the variations in computed transition-state free energies (Table 2), with propagation transition-state free energies showing less variation than chain-transfer transition-state free energies ($\Delta\Delta G^{\ddagger}_{P}$ = 3.4 kcal/mol versus $\Delta\Delta G^{\ddagger}_{CT}$ = 9.5 kcal/mol).

Individual kinetic parameters of several photoinduced thiol−ene polymerizations have been determined experimentally. Sivertz and Bowman, for example, have used rotating sector techniques to monitor thiol−ene reactions and photopolymerizations between various thiols and alkenes. Sivertz and co-workers have measured propagation and chain-transfer rates for addition of methyl and butyl mercaptan to 1-pentene, isoprene, and styrene.[24−28] More recently, Bowman and co-workers have investigated the kinetics of photoinitiated thiol−ene reactions between mercaptopropionates and derivatives of norbornene, allyl ethers, vinyl ethers, acrylates, and vinyl silanes.[33,36,37] In each study propagation and chain-transfer rates were obtained by fitting the experimental data to a kinetic model. With only one exception, computationally predicted rates of propagation and chain-transfer for the reaction of 1 with alkenes **2**−**5**, **7**−**9**, and **12** are of the same order of magnitude or within 1 order of magnitude as rates k_P and k_{CT} obtained experimentally for related thiol and alkene derivatives (see Table S7 of the Supporting Information for direct comparisons). The one exception where experimental and computationally predicted rates deviate by greater than 1 order of magnitude is the k_P of styrene (experimental, 10^9 M^{-1} s^{-1}; computational, 10^6 M^{-1} s^{-1}). It would be unlikely or coincidental for individual rate parameters predicted computationally to exactly reproduce those measured experimentally given the differences between the computational and experimental studies: computational investigations reported in this article involve unsubstituted alkene and thiol monomers modeled in the gas phase whereas experimental propagation and chain-transfer rates correspond to various derivatives of di-, tri-, and/or tetrasubstituted alkenes and thiols photopolymerized either in solution or in bulk with the data then fit to a kinetic model. Still, the general agreement between experimental rates and those predicted computationally, as well as computational benchmarking studies (Table 1), lend support to the methods used herein to model thiol−ene click reactions.

Of similar importance to absolute individual rate parameters of radical initiated thiol−ene click reactions is the ratio of propagation to chain-transfer rates, k_P/k_{CT}. As noted above, for those thiol−ene combinations where k_P/k_{CT} is much greater than 1.0 the chain-transfer step is rate limiting and the reaction rate is first order with respect to thiol concentration; when k_P/k_{CT} is much less than 1.0 the propagation step is rate limiting and the reaction rate is first order with respect to alkene concentration, and when k_P/k_{CT} is equal to 1.0 the reaction is expected to be half order with respect to both thiol and alkene concentrations. Computationally predicted ratios of k_P/k_{CT} are given in Table 4 along with k_P/k_{CT} ratios obtained from fitting experimental data.[24,27,33] As can be seen in Table 4 there is general agreement between computational and experimental k_P/k_{CT} ratios for thiol−ene reactions involving vinyl silane (<1.0), vinyl ether (∼1.2), propene (5.0), methacrylate, styrene, and butadiene (each ≫1.0). Theoretical k_P/k_{CT} ratios for norbornene and allyl ether, however, differ significantly from those obtained using experimental data. While direct comparisons between k_P/k_{CT} ratios obtained experimentally and those modeled computationally may be misleading given the above-mentioned differences between experimental and computational methods, the significant differences between experimental and theoretical k_P/k_{CT} ratios in the cases of norbornene and allyl ether warrant further investigation.

An experimental k_P/k_{CT} ratio of 1.0 has been determined for norbornene when experimental data is fit to a pseudo-steady-state kinetic model, implying equal rates of propagation and chain-transfer. Using the same procedure, an experimental k_P/k_{CT} ratio of 10 has been found for allyl ether, implying chain-transfer is the rate-limiting step. Computational results, however, suggest chain-transfer is limiting for norbornene while the propagation step is rate limiting in the case of allyl ether. The prediction that $k_P \approx 100k_{CT}$ for norbornene (**5**) is a direct reflection of the 2.9 kcal/mol difference in $\Delta G^{\ddagger}_{P}$ and $\Delta G^{\ddagger}_{CT}$. As stated earlier the low propagation barrier for addition of **1**$^{\bullet}$ to norbornene results from alleviation of ring strain. Once the thiyl radical has added to the C−C double bond of norbornene there is no similar driving force to lower the barrier to chain-transfer and, while the radical stabilization energy of the norbornene carbon-centered radical intermediate is low, chain-transfer is still predicted to be significantly rate limiting. To obtain a norbornene k_P/k_{CT} ratio of 1.0 would require a significantly lower chain-transfer barrier, which would appear unlikely given the generally good agreement between computational and experimental results. Allyl ether (**4**), on the other hand, is predicted to have the third highest propagation free energy barrier. Because thiyl addition to allyl ether is endergonic (ΔG_P° = 1.6 kcal/mol) and the allyl ether carbon-centered radical intermediate has the lowest radical stabilization energy, the chain-transfer barrier is predicted to be 0.7 kcal/mol lower than propagation. It is possible that the k_P/k_{CT} for allyl ether (**4**) could be closer to or even slightly greater than 1.0 given the average error of ±0.5 kcal/mol (Table 2) for the computational methods used in this study, however current computational analysis suggests the propagation step is rate limiting for the addition of alkyl thiyl radicals to allyl ether.

With the forward and reverse rates for propagation and chain-transfer steps predicted computationally (Table 4) it becomes possible to rank alkenes **2**−**13** in order of their reactivity with methyl mercaptan **1**. For six of the 12 alkenes (**5**−**8**, **10**, **12**) the chain-transfer step is rate limiting (k_{CT} > $100k_P$) and a steady-state assumption that the concentration of carbon-centered radical does not change with time can be expected to describe overall reaction kinetics reasonably well. Predicted propagation and chain-transfer rates for the remaining six alkenes (**2**−**4**, **9**, **11**, **13**) are within 2 orders of magnitude of each other. Furthermore, rates of reverse propagation (k_{-P}) are equal to or faster than rates of forward chain-transfer (k_{CT}) for all 12 alkenes investigated. An instructive example is provided by vinyl ether (**3**), for which k_P and k_{CT} are both predicted to be of the same order of magnitude (10^6 M^{-1} s^{-1}), while k_{-P} is 2 orders of magnitude

faster than both forward rates (10^8 s^{-1}). It is likely that a steady-state kinetic model will not accurately describe the overall reaction kinetics of thiol−ene click chemistry when k_P and k_{CT} are similar and k_{-P} is $\geq k_{CT}$[RSH], which is the case for alkenes **2**−**4**, **9**, **11**, and **13**.

The program Kintecus[66] was used to evaluate the kinetics of radical initiated thiol−ene click chemistry between methyl mercaptan and alkenes **2**−**13**. The program allows for rapid modeling of chemical reactions by numerically solving for concentrations of chemical species as a function of time given rate constants and initial concentrations of reactants for a series of chemical equations. Each thiol−ene reaction was modeled separately and both propagation and chain-transfer steps were treated as reversible. Calculated values of k_P, k_{-P}, k_{CT}, and k_{-CT} were input into the model along with initial concentrations of thiol, alkene, and initiator. The initial concentrations of thiol and alkene were taken to be 1.0 M and an initial concentration of generic photoinitiator "I" was chosen to be 0.001 M (0.1 mol %). The rate constant for photoinitiation was set to 1.0×10^{-5} M^{-1} s^{-1}, a value representative of the commonly used photoinitiator 2,2-dimethoxy-2-phenylacetophenone (DMPA) at low light intensity and moderate efficiency.[67] Rates for radical termination processes—coupling of two thiyl radicals, coupling of two carbon-centered radicals, and coupling of a thiyl radical with a carbon-centered radical—were each set to 1.0×10^8 M^{-1} s^{-1} in accordance with experimental termination rate constants.[36] Each thiol−ene reaction was simulated for a period of 600 min, while the concentrations of all chemical species (thiol, ene, thiyl radical, carbon-centered radical, thioether product, and initiator) were simultaneously monitored as a function of time. By normalizing with respect to initiation and termination kinetics, and forgoing any steady-state assumptions, a general model of the underlying influence of alkene structure on thiol−ene click reactions can be determined. Results from kinetic modeling are collectively plotted in Figure 9.

Figure 9 displays graphically the results of applying computationally predicted rate constants from Table 4 to a given set of thiol−ene reaction conditions. Choosing different reaction conditions (i.e., concentrations of thiol and ene or rates of photoinitiation and termination) influences the overall reaction kinetics for each thiol−ene system, however the relative order of reactivity across the 12 alkenes investigated remains unchanged across a wide range of inputs. Computational modeling predicts the order of reactivity of alkenes **2**−**13** with methyl mercaptan in radical initiated thiol−ene reactions shown in Figure 10. While experimental parameters (e.g., thiol−ene stoichiometry, solvent, diffusion, competitive chain-growth processes, specific thiol and ene substitution and solubility, etc.) will also play a role in overall thiol−ene kinetics, the predicted trend in reactivity is in good agreement with what has been observed experimentally.[10a,c,33] When coupled with thermodynamic (Table 2) and kinetic data (Table 4), these results provide significant insight into the underlying factors that control alkene reactivity. A comparison of maleimide (**13**) and methacrylate (**7**) provides a representative example. The predicted propagation rate for maleimide is an order of magnitude slower than that of methacrylate (10^5 versus 10^6 M^{-1} s^{-1}), and the two alkenes have similar predicted chain-transfer rates (both 10^3 M^{-1} s^{-1}), yet maleimide is predicted to be *more* reactive with methyl mercaptan than methacrylate is. The reason lies in the relative rates of reverse propagation, k_{-P}. Reverse propagation for methacrylate is an order of magnitude *faster* than chain-transfer, whereas for maleimide reverse propagation is slightly *slower* than chain-transfer. This can be further explained by comparing the relative heights of propagation step activation barriers and relative stabilities of carbon-centered radical intermediates along the reaction coordinates of maleimide and methacrylate, the propagation steps of which are similarly exergonic yet the notably high propagation step activation barrier for maleimide significantly disfavors reversibility relative to the lower propagation barrier for methacrylate. Fumarate (**11**) and propene (**2**) provide a similar example where the relative rates of k_{-P} must be taken into consideration in order to understand their relative overall reactivity. In general a high barrier to propagation and formation of a stable carbon-centered radical intermediate disfavors reverse propagation, whereas a low propagation barrier and less stable carbon-centered radical intermediate favors rapid reversibility of the propagation step. Note, however, that a very stable carbon-centered radical intermediate can considerably disfavor the chain-transfer step and significantly slow the overall reaction kinetics, as exemplified by butadiene (**8**) and acrylonitrile (**6**).

Given the significant role the reverse propagation rate k_{-P} can play in overall thiol−ene kinetics it is instructive to model overall reaction kinetics when considering propagation and chain-transfer steps to be irreversible. Modeling thiol−ene reactivity under identical reaction conditions as in Figure 9 with the exception that only forward rates (k_P and k_{CT}) are included yields different overall kinetics for 4 of the 12 alkenes; the reactivity of propene (**2**), vinyl ether (**3**), allyl ether (**4**), and

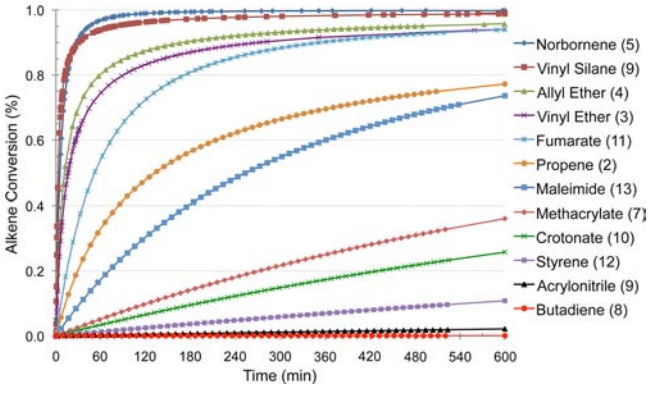

Figure 9. Results of kinetic modeling of photoinitiated thiol−ene click chemistry between methyl mercaptan (**1**) and alkenes **2**−**13** plotted as percent alkene conversion as a function of time. Reaction parameters used to model all thiol−ene reactions: $[CH_3SH]_0 = [alkene]_0 = 1.0$ M, $[initiator]_0 = 1.0$ mM, initiation rate $k_I = 1.0 \times 10^{-5}$ M^{-1} s^{-1}, radical−radical termination rates $k_t = 1.0 \times 10^8$ M^{-1} s^{-1}.

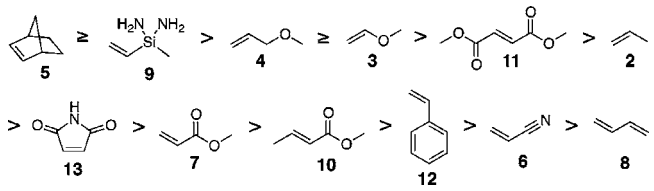

Figure 10. Predicted order of reactivity of alkenes **2**−**13** with methyl mercaptan **1**: norbornene ≥ vinyl silane > allyl ether ≥ vinyl ether > fumarate > propene > maleimide > methacrylate > crotonate > styrene > acrylonitrile > butadiene.

dx.doi.org/10.1021/ja305441d | J. Am. Chem. Soc. 2012, 134, 13804−13817

vinyl silane (**9**) increases when k_{-P} is not considered part of the overall kinetic scheme (see Figure S3 of the Supporting Information). This group also represents the only four alkenes studied for which the propagation step is endergonic (ΔG°_{P} = 0.4−2.1 kcal/mol), primarily due to their relative inability to stabilize their intermediate carbon-centered radical species. The overall reaction kinetics of the remaining 8 alkenes is essentially unchanged when k_{-P} is not included in the overall reaction scheme.

Modeling has therefore revealed the critically import role that the relative stability of the carbon-centered radical intermediate plays in determining overall reaction energetics and kinetics. In particular, the relative energy of the carbon-centered radical intermediate with respect to propagation and chain-transfer activation barriers determines the reversibility of the propagation step and whether that reversibility influences overall reaction kinetics. When k_{-P} is greater than or equal to k_P[ene] and k_{CT}[RSH] then reverse propagation directly influences the overall rate of the thiol−ene click reaction as the equilibrium of the rapidly reversible propagation step lies toward starting materials. This has been shown to be the case for propene (**2**), vinyl ether (**3**), allyl ether (**4**), and vinyl silane (**9**). Reversibility of the propagation step does not significantly influence overall reaction kinetics for the remaining 8 alkenes (**5**−**8** and **10**−**13**) where k_{-P} is less than k_P[ene] and k_{CT} is rate determining. Specific results will depend on the concentrations of thiol and alkene, however most thiol−ene click reactions are performed at relatively high concentrations or in bulk[10a,c−e] and the concentrations of 1.0 M used in this study can be considered representative. For these alkenes a pseudo-steady-state kinetic model wherein the concentration of radical species does not change over time would be expected to describe the overall reaction kinetics reasonably well. Such an assumption would not adequately describe the overall kinetics of thiol−ene reactions between alkane thiols and propene (**2**), vinyl ether (**3**), allyl ether (**4**), or vinyl silane (**9**). These results highlight the importance of obtaining a complete understanding of the reaction energetics in thiol−ene chemistry in order to fully understand and adequately model the kinetics of these complex step-growth radical processes. Computational studies such as those reported herein are especially helpful in this regard and can be of significant predictive power as the relative energetics of radical reactive intermediates can be difficult to obtain experimentally.

CONCLUSION

The energetics and kinetics of photoinitiated thiol−ene click reactions between methyl mercaptan **1** and a series of 12 alkenes (**2**−**13**) have been modeled at the CBS-QB3 level and are able to explain the influence of alkene structure on overall reactivity. The thiyl radical **1**$^{\bullet}$ has been shown to behave as an electrophile when adding to the C−C double bond of alkenes **2**−**13**. Propagation step activation barriers can not be directly correlated with any single electronic or structural property of the 12 alkenes investigated and are best described by a state correlation model wherein several electronic configurations are able to mix with and contribute to the overall propagation step activation barrier. The activation barrier for chain-transfer is found to be directly related to the ability of alkene substituents to stabilize the carbon-centered radical intermediate. Forward and reverse rate constants for propagation and chain-transfer steps between thiol **1** and alkenes **2**−**13** have been calculated from the results of electronic structure calculations and are found to be in good agreement with experimental rate constants for related thiol−ene reactions. Kinetic modeling of radical initiated reactions between thiol **1** and alkenes **2**−**13** under identical conditions has enabled the order of reactivity of the series of alkenes to be determined. Perhaps more importantly, kinetic analysis has revealed the importance of the stability of the carbon-centered radical intermediate, which directly influences not only the chain-transfer activation barrier but also the reversibility of the propagation step. It has been found that when the propagation step is endergonic and $k_{-P} > k_{CT}$[RSH] the rate of reverse propagation factors directly into the overall reaction kinetics. Small changes in alkene substitution can therefore have a significant impact on thiol−ene reactivity, not only through their influence on the rates of propagation and chain-transfer but also through their impact on the stability of the carbon-centered radical intermediate, which directly influences the relative rate constants k_P, k_{-P}, and k_{CT}. These results provide a more fundamental understanding of underlying influence of alkene functionality on the energetics, kinetics, and overall reactivity of a wide variety of alkenes in thiol−ene click chemistry. This understanding can be applied to further optimize and tailor the use of thiol−ene reactions in synthetic, materials, polymer, and biological chemistry, and can be particularly helpful for predicting and understanding outcomes of complex reactions involving several thiols and/or alkenes.

COMPUTATIONAL DETAILS

All calculations were performed with the Gaussian09 suite of programs.[68] Prior to geometry optimization to full convergence, potential energy surfaces of all structures were thoroughly explored by scanning all freely rotating dihedral angles at the HF/6-31G* (closed shell species) or UHF/6-31G* levels (open shell species) in order to locate their approximate global minimum energy conformations. Full geometry optimization, vibrational, and thermal analysis were then performed with the CBS-QB3 compound method.[39] CBS-QB3 calculations involve a DFT geometry optimization at the B3LYP/6-311G(2d,d,p) level followed by a series of higher level calculations designed to extrapolate to a complete basis set model. CBS-QB3 includes a "spin correction" term for open shell and radical species and has been shown to predict bond dissociation energies, enthalpies of formation, and adiabatic ionization potentials and electron affinities to within ±1.0 kcal/mol mean absolute deviation (MAD) from experimental data.[69] In the current study, benchmarking CBS-QB3 predicted reaction enthalpies to within ±0.5 MAD from experimental values for a series of five thiol−ene reactions and the bond dissociation of methyl mercaptan (see Table 1). Transition-state searches were performed by one of two methods: (1) performing relaxed potential energy surface scans of the bond coordinate(s) corresponding to bond breaking/formation, or (2) using the QST2 method.[70] Transition states were then refined using a Berny optimization with the CBS-QB3 method. Transition states were distinguished as having a single imaginary vibrational frequency corresponding to the vibrational mode connecting reactants and products. Optimizations of minima and transition states were performed in the gas phase at 1.0 atm pressure and 298.15 K. Adiabatic ionization potentials and electron affinities were calculated from the energies of the relaxed neutral molecule and corresponding relaxed ion at the CBS-QB3 level and include zero point and thermal corrections to 298.15 K. Singlet−triplet gaps were calculated at the CBS-QB3 level from the energy difference between energy minimized ground-state singlet and relaxed triplet structures of each alkene.

■ ASSOCIATED CONTENT

Supporting Information

Electrostatic density plots of alkenes **2**−**13**; relative energetics of *exo* and *endo* propagation and chain-transfer steps for norbornene (**5**); complete table of computed and experimental ionization potentials and electron affinities; plots of ΔH_{CT}° versus C−H and S−H transition-state bond distances; table of carbon-centered radical intermediate radical stabilization energies; complete tables of calculated transition-state entropies, pre-exponential factors, and activation energies used to determine k_P, k_{-P}, k_{CT}, and k_{-CT}; direct comparisons of experimental and calculated propagation and chain-transfer rate constants; plot of alkene conversion as a function of time when propagation and chain-transfer are considered irreversible; Cartesian coordinates of all stationary points reported herein and their absolute energies in hartrees; and complete ref 68. This material is available free of charge via the Internet at http://pubs.acs.org.

■ AUTHOR INFORMATION

Corresponding Author

bnorthrop@wesleyan.edu

Notes

The authors declare no competing financial interest.

■ ACKNOWLEDGMENTS

Acknowledgement is made to the donors of The American Chemical Society Petroleum Research Fund for partial support of this research through a research grant to B.H.N. We are grateful to the National Institutes of Health Doctoral Studies in Molecular Biophysics Training Grant 5 T32GM008271 for fellowship support to R.N.C. We thank Wesleyan University for computer time supported by the NSF under grant number CNS-0619508. We thank Profs. George A. Petersson and Reinhold Blumel for helpful discussions.

■ REFERENCES

(1) (a) Kold, H. C.; Finn, M. G.; Sharpless, K. B. *Angew. Chem., Int. Ed.* **2001**, *40*, 2004−2021. (b) Mose, J. E.; Moorhouse, A. D. *Chem. Soc. Rev.* **2007**, *36*, 1249−1262 and references therein.

(2) (a) Bock, V. D.; Hiemstra, H.; van Maarseveen, J. H. *Eur. J. Org. Chem.* **2006**, 51−68. (b) Hein, J. E.; Folkin, V. V. *Chem. Soc. Rev.* **2010**, *39*, 1302−1315.

(3) (a) Hawker, C. J.; Wooley, K. L. *Science* **2005**, *309*, 1200−1205. (b) Binder, W. H.; Sachsenhofer, R. *Macromol. Rapid Commun.* **2007**, *28*, 15−54. (c) Fournier, D.; Hoogenboom, R.; Schubert, U. S. *Chem. Soc. Rev.* **2007**, *36*, 1369−1380. (d) Lundberg, P.; Hawker, C. J.; Hult, A.; Malkoch, M. *Macromol. Rapid Commun.* **2008**, *29*, 998−1015. (e) Iha, R. K.; Wooley, K. L.; Nyström, A. M.; Burke, D. J.; Kade, M. J.; Hawker, C. J. *Chem. Rev.* **2009**, *109*, 5620−5686. (f) Golas, P. L.; Matyjaszewski, K. *Chem. Soc. Rev.* **2010**, *39*, 1338−1354.

(4) (a) Wu, P.; Feldman, A. K.; Nugent, A. K.; Hawker, C. J.; Scheel, A.; Voit, B.; Pyun, J.; Fréchet, J. M. J.; Sharpless, K. B.; Fokin, V. V. *Angew. Chem., Int. Ed.* **2004**, *43*, 3928−3932. (b) Malkoch, M.; Schleicher, K.; Drockenmuller, E.; Hawker, C. J.; Russell, T. P.; Wu, P.; Fokin, V. V. *Macromolecules* **2005**, *38*, 3663−3678. (c) Wu, P.; Malkoch, M.; Hunt, J. N.; Vestberg, R.; Kaltgrad, E.; Finn, M. G.; Fokin, V. V.; Sharpless, K. B.; Hawker, C. J. *Chem. Commun.* **2005**, 5775−5777. (d) Carlmark, A.; Hakwer, C. J.; Hult, A.; Malkoch, M. *Chem. Soc. Rev.* **2009**, *38*, 352−362. (e) Franc, G.; Kakkar, A. K. *Chem. Soc. Rev.* **2010**, *39*, 1536−1544.

(5) (a) Collman, J. P.; Devaraj, N. K.; Chidsey, C. E. D. *Langmuir* **2004**, *20*, 1051−1053. (b) Devaraj, N. K.; Miller, G. P.; Ebina, W.; Kakaradov, B.; Collman, J. P.; Kool, E. T.; Chidsey, C. E. D. *J. Am. Chem. Soc.* **2005**, *127*, 8600−8601. (c) Rozkiewicz, D. I.; Janczewski, D.; Verboom, W.; Ravoo, B. J.; Reinhoudt, D. N. *Angew. Chem., Int. Ed.* **2006**, *118*, 5418−5422. (d) Nandivada, H.; Jiang, X.; Lahann, J. *Adv. Mater.* **2007**, *19*, 2197−2208.

(6) (a) Kolb, H. C.; Sharpless, K. B. *Drug Discov. Today* **2003**, *8*, 1128−1137. (b) Sharpless, K. B.; Manetsch, R. *Expert Opin. Drug Dis.* **2006**, *1*, 525−538. (c) Mamidyala, S. K.; Finn, M. G. *Chem. Soc. Rev.* **2010**, *39*, 1252−1261.

(7) (a) Lee, L. V.; Mitchell, M. L.; Huang, S.-J.; Fokin, V. V.; Sharpless, K. B.; Wong, C.-H. *J. Am. Chem. Soc.* **2003**, *125*, 9588−9589. (b) Manetsch, R.; Krasinski, A.; Radic, Z.; Raushel, J.; Taylor, P.; Sharpless, K. B.; Kolb, H. C. *J. Am. Chem. Soc.* **2004**, *126*, 12809−12818. (c) Whiting, M.; Muldoon, J.; Lin, Y. C.; Silverman, S. M.; Lindstrom, W.; Olson, A. J.; Klob, H. C.; Finn, M. G.; Sharpless, K. B.; Elder, J. H.; Fokin, V. V. *Angew. Chem., Int. Ed.* **2006**, *45*, 1435−1439.

(8) (a) Speers, A. E.; Adam, G. C.; Cravatt, B. F. *J. Am. Chem. Soc.* **2003**, *125*, 4686−4687. (b) Baskin, J. M.; Prescher, J. A.; Laughlin, S. T.; Nicholas, J. A.; Chang, P. V.; Miller, I. A.; Lo, A.; Codelli, J. A.; Bertozzi, C. R. *Proc. Natl. Acad. Sci. U.S.A.* **2007**, *104*, 16793−16797. (c) Laughlin, S. T.; Baskin, J. M.; Amacher, S. J.; Bertozzi, C. R. *Science* **2008**, *320*, 664−667. (d) Jewett, J. C.; Bertozzi, C. R. *Chem. Soc. Rev.* **2010**, *39*, 1272−1279.

(9) (a) Aprahamian, I.; Miljanic, O. S.; Dichtel, W. R.; Isoda, K.; Yasuda, T.; Kato, T.; Stoddart, J. F. *Bull. Chem. Soc. Jpn.* **2007**, *80*, 1856−1869. (b) Braunschweig, A. B.; Dichtel, W. R.; Miljanic, O. S.; Olson, M. A.; Spruell, J. M.; Kahn, S. I.; Heath, J. R.; Stoddart, J. F. *Chem. Asian J.* **2007**, *2*, 634−647. (c) Haenni, K. D.; Leigh, D. A. *Chem. Soc. Rev.* **2010**, *39*, 1240−1251.

(10) For recent reviews of thiol-ene click chemistry see: (a) Hoyle, C. E.; Lee, T. Y.; Roper, T. *J. Polym. Sci. Part A* **2004**, *42*, 5301−5338. (b) Dondoni, A. *Angew. Chem., Int. Ed.* **2008**, *47*, 8995−8997. (c) Hoyle, C. E.; Bowman, C. N. *Angew. Chem., Int. Ed.* **2010**, *49*, 1540−1573. (d) Hoyle, C. E.; Lowe, A. B.; Bowman, C. N. *Chem. Soc. Rev.* **2010**, *39*, 1355−1387. (e) Kade, M. J.; Burke, D. J.; Hawker, C. J. *J. Polym. Sci. Part A* **2010**, *48*, 743−750.

(11) Posner, T. *Ber. Dtsch. Chem. Ges.* **1905**, *38*, 646−657.

(12) Jacobine, A. F. Experimental and Analytical Methods for the Investigation of Radiation Curing. In *Radiation Curing in Polymer Science and Technology III*; Fouassier, J. D., Rabek, J. F., Eds.; Elsevier: London, 1993; pp 219−268.

(13) Griesbaum, K. *Angew. Chem., Int. Ed. Engl.* **1970**, *9*, 273−287.

(14) (a) Killops, K. L.; Campos, L. M.; Hawker, C. J. *J. Am. Chem. Soc.* **2008**, *130*, 5062−5064. (b) Montañez, M. I.; Campos, L. M.; Antoni, P.; Hed, Y.; Walter, M. V.; Krull, B. T.; Khan, A.; Hult, A.; Hakwer, C. J.; Malkoch, M. *Macromolecules* **2010**, *43*, 6004−6013. (c) Antoni, P.; Robb, M. J.; Camposs, L. M.; Montañez, M.; Hult, A.; Malmström, E.; Malkoch, M.; Hawker, C. J. *Macromolecules* **2010**, *43*, 6625−6631.

(15) (a) Hagberg, E. C.; Malkoch, M.; Ling, Y.; Hawker, C. J.; Carter, K. R. *Nano Lett.* **2007**, *7*, 233−237. (b) Khire, V. S.; Yi, Y.; Clark, N. A.; Bowman, C. N. *Adv. Mater.* **2008**, *20*, 3308−3313. (c) Campos, L. M.; Meinel, I.; Guino, R. G.; Schierhorn, M.; Gupta, N.; Stucky, G. D.; Hawker, C. J. *Adv. Mater.* **2008**, *20*, 3728−3733.

(16) (a) Cygan, Z. T.; Cabral, J. T.; Beers, K. L.; Amis, E. J. *Langmuir* **2005**, *21*, 3629−3634. (b) Cabral, J. T.; Hudson, S. D.; Harrison, C.; Douglas, J. F. *Langmuir* **2004**, *20*, 10020−10029. (c) Harrison, C.; Cabral, J.; Stafford, C. M.; Karim, A.; Amis, E. J. *J. Micromech. Microeng.* **2008**, *14*, 153−158. (d) Hung, L. H.; Lin, R.; Lee, A. P. *Lab Chip* **2008**, *8*, 983−987.

(17) (a) Khire, V. S.; Benoit, D. S. W.; Anseth, K. S.; Bowman, C. N. *J. Polym. Sci. Part A* **2006**, *44*, 7027−7039. (b) Besson, E.; Gue, A. M.; Sudor, J.; Korri-Youssoufi, H.; Jaffrezic, N.; Tardy, J. *Langmuir* **2006**, *22*, 8346−8352. (c) Khire, V. S.; Harant, A. W.; Watkins, A. W.; Anseth, K. S.; Bowman, C. N. *Macromolecules* **2006**, *39*, 5081−5086. (d) Harant, A. W.; Khire, V. S.; Thibodaux, M. S.; Bowman, C. N. *Macromolecules* **2006**, *39*, 1461−1466. (e) Jonkheijm, P.; Weinrich, D.; Köhn, M.; Engelkamp, H.; Christianen, P. C. M.; Kuhlmann, J.; Maan, J. C.; Nüsse, D.; Schroeder, H.; Wacker, R.; Breinbauer, R.; Niemeyer, C. M.; Waldmann, H. *Angew. Chem., Int. Ed.* **2008**, *47*, 4421−4424. (f) Gupta, N.; Lin, B. F.; Campos, L. M.; Dimitriou, M. D.; Hikita, S.

T.; Treat, N. D.; Tirrell, M. V.; Clegg, D. O.; Kramer, E. J.; Hawker, C. J. *Nature Chem.* **2010**, *2*, 138−145.
(18) (a) Bhargava, R.; Wang, S. Q.; Koenig, J. L. *Macromolecules* **1999**, *32*, 2748−2760. (b) Park, S. H.; Xia, Y. *Langmuir* **1999**, *15*, 266−273. (c) Natarajan, L. V.; Shepherd, C. K.; Brandelik, D. M.; Sutherland, R. L.; Chandra, S.; Tondiglia, V. P.; Tomlin, D.; Bunning, T. J. *Chem. Mater.* **2003**, *15*, 2477−2484.
(19) (a) Elbert, D. L.; Pratt, A. B.; Lutolf, M. P.; Halstenberg, S.; Hubbell, J. A. *J. Controlled Release* **2011**, *76*, 11−25. (b) Hubbell, J. A.; Lutolf, M. P. *Biomacromolecules* **2003**, *4*, 713−722. (c) Rydholm, A. E.; Reddy, S. K.; Anseth, K. S.; Bowman, C. N. *Biomacromolecules* **2006**, *7*, 2827−2836. (d) Polizzotti, B. D.; Fairbanks, B. D.; Anseth, K. S. *Biomacromolecules* **2008**, *9*, 1084−1087. (e) DeForest, C. A.; Polizzotti, B. D.; Anseth, K. S. *Nat. Mater.* **2009**, *8*, 659−664.
(20) (a) Gao, Y.; Eguchi, A.; Kakehi, K.; Lee, Y. C. *Org. Lett.* **2004**, *6*, 3457−3460. (b) Tucker-Schwartz, A. K.; Farrell, R. A.; Garrell, R. L. *J. Am. Chem. Soc.* **2011**, *133*, 11026−11029.
(21) (a) You, L.; Schlaad, H. *J. Am. Chem. Soc.* **2006**, *128*, 13336−13337. (b) Geng, Y.; Discher, D. E.; Justynska, J.; Schlaad, H. *Angew. Chem., Int. Ed.* **2006**, *45*, 7578−7581. (c) Chen, G.; Amajjahe, S.; Stenzel, M. H. *Chem. Commun.* **2009**, 1198−1200.
(22) Wittrock, S.; Becker, T.; Kunz, H. *Angew. Chem., Int. Ed.* **2007**, *46*, 5226−5230.
(23) Ghosh, S. S.; Koa, P. M.; McCue, A. W.; Chappelle, H. L. *Bioconjugate Chem.* **1990**, *1*, 71−76.
(24) Back, R.; Trick, G.; McDonald, C.; Sivertz, C. *Can. J. Chem.* **1954**, *32*, 1078−1091.
(25) Onyszchuk, M.; Sivertz, C. *Can. J. Chem.* **1955**, *33*, 1034−1042.
(26) Sivertz, C.; Andrews, W.; Elsdon, W.; Graham, K. *J. Polym. Sci.* **1956**, *19*, 587−588.
(27) Sivertz, C. *J. Phys. Chem.* **1959**, *63*, 34−38.
(28) Graham, D. M.; Mieville, R. L.; Pallen, R. H.; Sivertz, C. *Can. J. Chem.* **1964**, *42*, 2250−2255.
(29) Morgan, C. R.; Magnotta, F.; Ketley, A. D. *J. Polym. Sci. Polym. Chem. Ed.* **1977**, *15*, 627−645.
(30) Ito, O.; Matsuda, M. *J. Org. Chem.* **1984**, *49*, 17−20.
(31) Cramer, N. B.; Bowman, C. N. *J. Polym. Sci. Part A* **2001**, *39*, 3311−3319.
(32) Cramer, N. B.; Davies, T.; O'Brien, A. K.; Bowman, C. N. *Macromolecules* **2003**, *36*, 4631−4636.
(33) Cramer, N. B.; Reddy, S. K.; O'Brien, A. K.; Bowman, C. N. *Macromolecules* **2003**, *36*, 7964−7969.
(34) Roper, T. M.; Guymon, C. A.; Jönsson, E. S.; Hoyle, C. E. *J. Polym. Sci. Part A* **2004**, *42*, 6283−6298.
(35) Cramer, N. B.; Reddy, S. K.; Cole, M.; Hoyle, C.; Bowman, C. N. *J. Polym. Sci. Part A* **2004**, *24*, 5817−5825.
(36) Reddy, S. K.; Cramer, N. B.; Bowman, C. N. *Macromolecules* **2006**, *39*, 3673−3680.
(37) Reddy, S. K.; Cramer, N. B.; Bowman, C. N. *Macromolecules* **2006**, *39*, 3681−3687.
(38) Okay, O.; Bowman, C. N. *Macromol. Theory Simul.* **2005**, *14*, 267−277.
(39) (a) Nyden, M. R.; Petersson, G. A. *J. Chem. Phys.* **1981**, *75*, 1843−1862. (b) Petersson, G. A.; Al-Laham, M. A. *J. Chem. Phys.* **1991**, *94*, 6081−6090. (c) Petersson, G. A.; Tensfeldt, T.; Montgomery, J. A. *J. Chem. Phys.* **1991**, *94*, 6091−6101. (d) Montgomery, J. A.; Ochterski, J. W.; Petersson, G. A. *J. Chem. Phys.* **1994**, *101*, 5900−5909.
(40) Good, W. D.; Lacina, J. L.; McCullough, J. P. *J. Phys. Chem.* **1961**, *65*, 2229−2231.
(41) Furuyama, S.; Golden, D. M.; Benson, S. W. *J. Chem. Thermodyn.* **1969**, *1*, 363−375.
(42) Hubbard, W. N.; Good, W. D.; Waddington, G. *J. Phys. Chem.* **1958**, *62*, 614−617.
(43) Prosen, E. J.; Maron, F. W.; Rossini, F. D. *J. Res. NBS* **1951**, *46*, 106−112.
(44) Geller, B. E. *Russ. J. Phys. Chem.* **1961**, *35*, 542−564.
(45) McCullough, J. P.; Hubbard, W. N.; Frow, F. R.; Hossenlopp, I. A.; Waddington, G. *J. Am. Chem. Soc.* **1957**, *79*, 561−566.
(46) Hubbard, W. N.; Waddington, G. *Recl. Trav. Chim. Pays/Bas* **1954**, *73*, 910.
(47) McCullough, J. P.; Finke, H. L.; Hubbard, W. N; Todd, S. S.; Messerly, J. F.; Douslin, D. R.; Waddington, G. *J. Phys. Chem.* **1961**, *65*, 784−791.
(48) Nicovich, J. M.; Kreutter, K. D.; van Dijk, C. A.; Wine, P. H. *J. Phys. Chem.* **1992**, *96*, 2518−2528.
(49) Campos, L. M.; Killops, K. L.; Sakai, R.; Paulusse, J. M. J.; Damiron, D.; Drockenmuller, E.; Messmore, B. W.; Hawker, C. J. *Macromolecules* **2008**, *41*, 7063−7070.
(50) Uygun, M.; Tasdelen, M. A.; Yagci, Y. *Macromol. Chem. Phys.* **2010**, *211*, 103−110.
(51) (a) Tedder, J. M.; Walton, J. C. *Acc. Chem. Res.* **1976**, *9*, 183−191. (b) Tedder, J. M.; Walton, J. C. *Adv. Phys. Org. Chem.* **1978**, *18*, 51−86. (c) Tedder, J. M. *Angew. Chem., Int. Ed.* **1982**, *21*, 401−410.
(52) Giese, B. *Angew. Chem., Int. Ed.* **1983**, *22*, 753−764.
(53) Fischer, H.; Radom, L. *Angew. Chem., Int. Ed.* **2001**, *40*, 1340−1371.
(54) See, for example: (a) Houk, K. N.; Paddon-Row, M. N.; Spellmeyer, D. C.; Rondan, N. G.; Nagase, S. *J. Org. Chem.* **1986**, *51*, 2874−2879. (b) Gonzales, C.; Sosa, C.; Schlegel, H. B. *J. Phys. Chem.* **1989**, *93*, 2534−2440. (c) Zipse, H.; He, J.; Houk, K. N.; Giese, B. *J. Am. Chem. Soc.* **1991**, *113*, 4324−4325. (d) Wong, M. W.; Pross, A.; Radom, L. *J. Am. Chem. Soc.* **1994**, *116*, 6248−6292. (e) Arnaud, R.; Bugaud, N.; Vetere, V.; Barone, V. *J. Am. Chem. Soc.* **1998**, *120*, 5733−5740. (f) Lalevee, J.; Allonas, X.; Fouassier, J. P. *J. Phys. Chem. A* **2004**, *108*, 4326−4334. (g) Gómez-Balderas, R.; Coote, M. L.; Henry, D. J.; Radom, L. *J. Phys. Chem. A* **2004**, *108*, 2874−2883. (h) Lalevee, J.; Allonas, X.; Fouassier, J. P.; Rinaldi, D.; Lopez, M. F. R.; Rivail, J. L. *Chem. Phys. Lett.* **2005**, *415*, 202−205.
(55) Hammond, G. S. *J. Am. Chem. Soc.* **1955**, *77*, 334−338.
(56) Electron density plots for alkenes **2**−**13** have been calculated and are presented as Figure S1 of the Supporting Information.
(57) It should be noted that a thiyl radical can add to the *exo* or *endo* face of the double bond of norbornene. Activation parameters reported in Table 2 refer to *exo* addition. Addition to the *endo* face is predicted to require $\Delta G^{\ddagger}_{p}$ = 11.1 kcal/mol and is therefore not considered as *exo* addition is favored by 4.2 kcal/mol. Full results, including alternative modes of chain-transfer, are given in Scheme S1 of the Supporting Information.
(58) Evans, M. G.; Polanyi, M. *Trans. Faraday Soc.* **1938**, *34*, 11−24.
(59) For reviews of the curve-crossing model see: (a) Pross, A.; Shaik, S. S. *Acc. Chem. Res.* **1983**, *16*, 363−370. (b) Shaik, S.; Shurki, A. *Angew. Chem., Int. Ed.* **1999**, *38*, 586−625.
(60) For examples of the curve-crossing model applied to radical addition to alkenes see: (a) Wong, M. W.; Pross, A.; Radom, L. *J. Am. Chem. Soc.* **1993**, *115*, 11050−11051. (b) Salikhov, A.; Fischer, H. *Theor. Chem. Acc.* **1997**, *96*, 114−1121. (c) Zytowski, T.; Fischer, H. *J. Am. Chem. Soc.* **1997**, *119*, 12869−12878. (d) Donahue, N. M.; Clarke, J. S.; Anderson, J. G. *J. Phys. Chem. A* **1998**, *102*, 3923−3933. (e) Donahue, N. M. *J. Phys. Chem. A* **2001**, *105*, 1489−1497. (f) Lalevée, J.; Allonas, X.; Fouassier, J.-P. *J. Org. Chem.* **2005**, *70*, 814−819.
(61) (a) Pauling, L. *J. Am. Chem. Soc.* **1931**, *53*, 3225−3237. (b) Baird, N. C. *J. Chem. Educ.* **1977**, *54*, 291−293.
(62) (a) Pasto, D. J.; Krasnansky, R.; Zercher, C. *J. Org. Chem.* **1987**, *52*, 3062−3072. (b) Clark, K. B.; Wayner, D. D. M. *J. Am. Chem. Soc.* **1991**, *113*, 936−9365. (c) Henry, D. J.; Parkinson, C. J.; Mayer, P. M.; Radom, L. *J. Phys. Chem. A* **2001**, *105*, 6750−6756.
(63) (a) Wilt, J. W.; Kolewe, O. *J. Am. Chem. Soc.* **1965**, *87*, 2071−2072. (b) Wilt, J. W.; Kolewe, O.; Kraemer, J. F. *J. Am. Chem. Soc.* **1969**, *91*, 2624−2631. (c) Wetzel, D. M.; Brauman, J. I. *J. Am. Chem. Soc.* **1988**, *110*, 8333−8336.
(64) Chatgilialoglu, C.; Altieri, A.; Fischer, H. *J. Am. Chem. Soc.* **2002**, *124*, 12816−12823.
(65) McQuarrie, D. A.; Simon, J. D. Chemical Kinetics I: Rate Laws. *Physical Chemistry: A Molecular Approach*; University Science Books: Sausalito, CA, 1997; pp 1165−1169.
(66) Ianni, J. C. *Kintecus*, version 3.82, 2005; www.kintecus.com.

(67) DMPA is used here as a model initiator as it is one of the most commonly employed cleavage-type photoinitiators used in thiol−ene chemistry. Typical initiation rates for DMPA range from 10^{-6} to 10^{-3} M^{-1} s^{-1}, see: Lovestead, T. M.; Berchtold, K. A.; Bowman, C. N. *Macromol. Theory. Simul.* **2002**, *11*, 729−738. The initiation rate was intentionally chosen to be toward the low end of this range, and the initiator concentration was likewise relatively low, so that the formation and concentration of thiyl radical **1**$^{\bullet}$ would be dominated by propagation and chain-transfer kinetics rather than initiation.
(68) Frisch, M. J. et al. *Gaussian 09*, Revision A.1 (see the Supporting Information for the full reference).
(69) Wood, G. P.; Radom, L.; Petersson, G. A.; Barnes, E. C.; Frisch, M. J. *J. Phys. Chem.* **2006**, *125*, 094106−094106−16.
(70) Peng, C.; Ayala, P. Y.; Schlegel, H. B.; Frisch, M. J. *J. Comput. Chem.* **1996**, *17*, 49−56.